ELSEVIER

Thermochimica Acta 330 (1999) 65–73

thermochimica acta

Complex heat capacity measurements by TMDSC. Part 2. Algorithm for amplitude and phase angle correction

M. Merzlyakov, C. Schick*

Department of Physics, University of Rostock, Universitaetsplatz 3, D-18051 Rostock, Germany

Received 29 October 1998; accepted 8 January 1999

Abstract

To treat data from temperature modulated differential scanning calorimetry (TMDSC) in terms of complex heat capacity, one should know heat transfer and apparatus influences on experimental results. Concise theoretical model for power compensated DSC is given, which includes description of most important heat transfer paths and apparatus effects. Estimations for real experimental conditions are made. An algorithm to determine parameters for calibration to exclude heat transfer and apparatus effects is proposed. This allows to increase upper frequency limit and accuracy of TMDSC measurements. Based on theoretical results the key points of the correction and some experimental evidence are discussed.

Keywords: Complex heat capacity; Thermal conductivity; TMDSC; Calibration; Heat transfer; Phase angle

1. Introduction

Besides other dynamic calorimetric methods like AC [1–3] and 3ω [4,5], temperature modulated differential scanning calorimetry (TMDSC), introduced by Reading [6], gives a possibility to measure complex heat capacity [7,8]. Basic prerequisite for complex heat capacity determination is the linear response, which was discussed in detail in part 1 of this paper [9]. It is well understood however that the value for complex heat capacity being given by the ratio between measured heat flow rate and heating rate should be corrected for heat transfer effects. Such phase and amplitude calibration was discussed by different authors, e.g. [10–12], with the assumption of negligible temperature gradient inside the sample. But this temperature gradient can be significant especially in case of low thermal conducting materials, e.g. polymers. Influence of the sample thermal conductivity on heat capacity determination in TMDSC was studied by Schenker et al. [13]. Sophisticated mathematical model including influence of temperature gradient inside the sample has been proposed by Lacey et al. [14] for the heat flux DSC. However, there are some general difficulties to apply theoretical models: parameters for calibration are unknown or change in unknown way during the measurement. Although in some particular cases such as in glass transition, it is possible to apply empirical algorithm for the correction when heat capacity is complex and changes during transition [15], the question how to correct measured data for heat transfer effect in general case is still open.

*Corresponding author. Tel.: +49-381-498-1644; fax: +49-381-498-1626; e-mail: christoph.schick@physik.uni-rostock.de

0040-6031/99/$ – see front matter
PII: S0040-6031(99)00020-9

In the following paper, first we try to take into consideration all important contributions to heat transfer influences on measured signal in case of power compensated DSC. Parallel to theoretical model some estimations for real experimental conditions are given. After that apparatus effects are discussed and a method to eliminate them is proposed (by apparatus effects we imply influences on measurements from measuring unit and electronics itself such as their asymmetry, time constants and so on). Finally, an algorithm to determine calibration parameters and calibration itself is proposed.

2. TMDSC data treatment

Detailed description of the data treatment for TMDSC measurements is given in [6,16]. If some heat flow rate $\Phi(t)$ is measured under given heating rate $q(t)$, then after Fourier transform $F[f](\omega)=(f(t),e^{i(\omega,t)})$ [17], one can write (see also [9]):

$$F[C](\omega) = \frac{F[\Phi](\omega)}{F[q](\omega)} = m \cdot c_{\text{eff}}(\omega). \tag{1}$$

One can treat this ratio as an effective or apparent frequency dependent heat capacity $c_{\text{eff}}(\omega)$, where m is the sample mass. But, complex specific heat capacity of the sample $c_p(\omega)$ differs from this ratio, because in reality measured heat flow rate $\Phi(t)$ is not the heat flow rate into the sample $\Phi_s(t)$ and measured temperature, as well as measured heating rate $q(t)$ is not the sample temperature and sample heating rate $q_s(t)$. Since the behaviour of DSC is linear [18], one can connect true and measured values by convolution product with Green's functions [11], so that $\Phi_s(t)=\hat{G}_1(t)\times\Phi(t)$ and $q_s(t)=\hat{G}_2(t)\times q(t)$. After Fourier transform these relations become

$$F[\Phi_s](\omega) = F[G_1](\omega) \cdot F[\Phi](\omega), \tag{2}$$

$$F[q_s](\omega) = F[G_2](\omega) \cdot F[q](\omega), \tag{3}$$

where now $F[G_1](\omega)$ and $F[G_2](\omega)$ are some frequency dependent complex factors. Then, complex specific heat capacity of the sample $c_p(\omega)$ can be written as

$$m \cdot c_p(\omega) \equiv \frac{F[\Phi_s](\omega)}{F[q_s](\omega)} = \frac{F[G_1](\omega)}{F[G_2](\omega)} \frac{F[\Phi](\omega)}{F[q](\omega)}, \tag{4}$$

where m is the sample mass. When some heating rate with periodic part $q(t)=\text{Re}(A_q \cdot e^{-i\omega t})$ of amplitude A_q and angular frequency ω is applied to the sample, periodic part of heat flow rate $\Phi(t)=\text{Re}(A_\Phi \cdot e^{-i(\omega t-\epsilon)})$ of amplitude A_Φ and phase lag ϵ is induced and Eq. (4) becomes

$$m \cdot c_p(\omega) \equiv \frac{F[G_1](\omega)}{F[G_2](\omega)} \frac{A_\Phi}{A_q} e^{i\epsilon} = B(\omega) \frac{A_\Phi}{A_q} e^{i\epsilon}, \tag{5}$$

where $B(\omega)=|B(\omega)| \cdot e^{-\phi(\omega)}$ is some calibration factor which contains heat transfer and apparatus influences on sample heat capacity measurement. Note that not only modulus but also argument $\phi(\omega)$ of this calibration factor depends on frequency.

In the following specific complex heat capacity of the sample $c_p(\omega)$ is denoted as c_p only. Different possible apparent or effective heat capacities of the sample or other systems are denoted as C_i for total values and $c_i=C_i/m$ for specific values, where i is the corresponding sub-index and m is the sample mass. We also assume that the conditions of linearity and stationarity are fulfilled, see [9]. Under linear conditions one can separate underlying and periodic parts of signal. Temperature oscillations can be represented as $T(t)=A_T \cdot e^{-i\omega t}$ and heating rate oscillations as $q(t) \equiv \dot{T}(t) = -i\omega \cdot T(t)$. Any possible transition in the sample is allowed.

3. Influence of heat transfer

Consider a sample with an aluminium pan placed in the oven, as shown in Fig. 1(a). Disc shaped sample is 5.8 mm in diameter and about 0.1–1 mm thickness depending on the mass of polymer sample which is commonly in range 2–25 mg. Thermal conductivity of aluminium ($\kappa_{\text{Al}} \approx 210\ \text{W m}^{-1}\ \text{K}^{-1}$) is usually three order of magnitude larger than that of the polymers (e.g. thermal conductivity of poly(ether ether ketone) $\kappa_{\text{PEEK}} \approx 0.26\ \text{W m}^{-1}\ \text{K}^{-1}$, of polystyrene $\kappa_{\text{PS}} \approx 0.15\ \text{W m}^{-1}\ \text{K}^{-1}$) and the thickness of the pan walls is 0.1 mm. Under such conditions one can neglect temperature gradient in the aluminium pan and consider that sample is heated from both surfaces so that effective sample thickness d is in range 0.05–0.5 mm. Comparing this with 5.8 mm diameter in good approximation one can represent temperature oscillations in

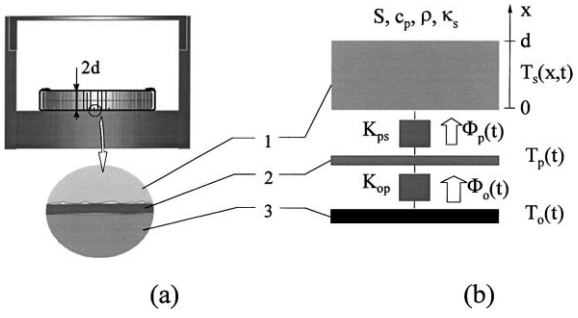

Fig. 1. The schematic view of the oven (a) and its block diagram (b). (1) sample, (2) pan, (3) oven.

the sample as plane waves and discuss only one-dimensional system. Sample being in semi-crystalline state or in high viscosity melt has never ideal thermal contact with pan – only few points have direct contact with pan, others have contact via air, as shown in Fig. 1(a). Then one should introduce an effective thermal contact K_{ps} between sample surface and pan. This thermal contact can change drastically during the measurements, e.g. when a nice ''wet contact'' which was in the melt is destroyed by contraction during crystallisation and large part of the sample surface looses the direct contact with pan. Thermal contact between the pan and the oven K_{op} is also mainly via an air layer, because the pan and the oven have direct contact, strictly speaking, only in three points. But this K_{op} is independent on sample properties and mainly determined by temperature and type of purge gas (usually nitrogen). This effective thermal contact includes also heat flow through ambient gas around the upper side of the pan, which is, however, much smaller than the heat coming through the bottom of the pan. Schematically, representation of the sample–pan–oven system is shown in Fig. 1(b), where $T_s(x,t)$ is the sample temperature, $T_p(t)$ the pan temperature, $T_o(t)$ the oven temperature, κ_s the thermal conductivity of the sample, ρ the sample density, c_p the specific heat capacity of the sample, and S is the area of the surface $x=0$. In case when κ_s, ρ, c_p do not depend on x, t, T_s heat transfer equation without heat sources can be written as

$$\frac{\partial T_s}{\partial t} = \chi \frac{\partial^2 T_s}{\partial x^2}, \tag{6}$$

where $\chi = \kappa_s/(\rho \cdot c_p)$ is the thermal diffusivity. When the temperature oscillation of the sample surface $x=0$ is given as $T_s(0,t) = A_{T_s} \cdot e^{-i\omega t}$ one can look for the solution of Eq. (6) in form $T_s(x,t) = A_{T_s} \cdot e^{-i(\omega t+kx)}$, where k is the wave number. In this case $\partial T_s/\partial t = -i\omega \cdot A_{T_s} \cdot e^{-i(\omega t+kx)}$ and $\partial^2 T_s/\partial x^2 = -k^2 \cdot A_{T_s} \cdot e^{-i(\omega t+kx)}$. Then according to Eq. (6) $i\omega = \chi k^2$, $k = \pm\sqrt{\omega/|\chi|}\exp\{(i/2)\arg(i\omega/\chi)\}$. Designate for short $\alpha = \sqrt{\omega/|\chi|}\exp\{(i/2)\arg(-i\omega/\chi)\}$. Finally, the temperature oscillation inside the sample can be written as

$$T_s(x,t) = A_{T_s} \cdot e^{-i\omega t}(A \cdot e^{-\alpha \cdot x} + B \cdot e^{\alpha \cdot x}), \tag{7}$$

where factors A and B are determined by boundary conditions. One of these conditions is that at $x=0$ temperature oscillation equals $T_s(0,t) = A_{T_s} \cdot e^{-i\omega t}$, so that from Eq. (7):

$$A + B = 1. \tag{8}$$

On the other hand there is no heat flow through the sample surface $x=d$ (because this surface is actually in the middle of the sample heated from both sides), i.e.

$$\Phi_s(d,t) = -\kappa_s \cdot S \left.\frac{\partial T_s}{\partial x}\right|_{x=d} = 0, \tag{9}$$

where $\Phi_s(x,t)$ denotes the heat flow inside the sample. Further, one can write $\partial T_s/\partial x = A_{T_s} \cdot e^{-i\omega t}(-A \cdot \alpha \cdot e^{-\alpha \cdot x} + B \cdot \alpha \cdot e^{\alpha \cdot x})$ and using Eq. (9) one can obtain $A \cdot e^{-\alpha \cdot d} = B \cdot e^{\alpha \cdot d}$, or $B = A \cdot e^{-2\alpha \cdot d}$. Then substituting this in Eq. (8) one can get: $A(1+e^{-2\alpha \cdot d}) = 1$, or $A = 1/(1 + e^{-2\alpha \cdot d})$. Finally, heat flow through the surface $x=0$ can be written as

$$\begin{aligned}\Phi_s(0,t) &= -\kappa_s \cdot S \left.\frac{\partial T}{\partial x}\right|_{x=0} \\ &= -\kappa_s \cdot S \cdot A_{T_s} e^{-i\omega t} \alpha \frac{-1 + e^{-2\alpha \cdot d}}{1 + e^{-2\alpha \cdot d}} \\ &= \kappa_s \cdot S \cdot A_{T_s} e^{-i\omega t} \alpha \tanh(\alpha \cdot d).\end{aligned} \tag{10}$$

This heat flow equals to the heat flow rate into the sample, $\Phi_p(t)$, Then one can formally rewrite Eq. (10) as

$$\Phi_p(t) = -C_\alpha \cdot i\omega \cdot T_s(0,t), \tag{11}$$

where C_α is the apparent heat capacity of the sample at the surface $x=0$ and equals

$$C_\alpha \equiv -\frac{1}{i\omega} \kappa_s \cdot S \cdot \alpha \tanh(\alpha \cdot d). \tag{12}$$

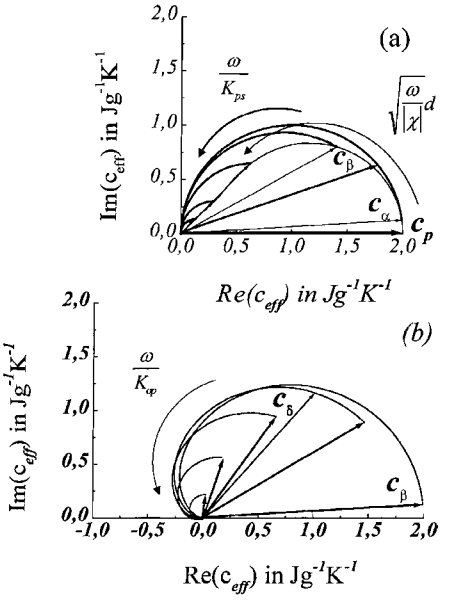

Fig. 2. (a) Polar plot showing the dependence of apparent heat capacity C_α on parameter $\sqrt{(\omega/|\chi|)}d$. On diagram specific heat capacity is set to real value and equals to 2 J g^{-1} K^{-1} ($c_p(\omega)$ can be complex in general case). During the change of parameter $\sqrt{(\omega/|\chi|)}d$, the end of the vector C_α follows the curve determining phase angle and modulus of C_α. Analogous happens with vector C_β during changes of $\omega/K_{\rm ps}$ and on diagram (b) with vector C_δ during changes of parameter $\omega/K_{\rm op}$.

Fig. 2(a) shows C_α dependence on parameter $\sqrt{(\omega/\chi)}d$. When the sample is very thin or modulation frequency is very low or sample thermal conductivity is very high, all sample parts can follow temperature modulation and apparent heat capacity C_α equals to sample heat capacity, in other words $C_\alpha \to m{\cdot}c_p$ at $\sqrt{(\omega/\chi)}d \to 0$. On the contrary, at $\sqrt{(\omega/\chi)}d \to \infty$, temperature waves can propagate only through the thin surface layer of the sample so that $C_\alpha \to 0$ and $\arg(C_\alpha) \to \pi/4 + (1/2)\arg(c_p)$ (note that in general case $\arg(c_p) \neq 0$). Estimation of temperature gradient influence on measured values is given in Table 1 for two sample masses m=2.5 mg and m=25 mg. The parameters for the calculations by Eq. (12) are the following: $t_{\rm p}$=1 min, S=53 mm^2, $\kappa_{\rm s}$=0.26 W m^{-1} K^{-1}, ρ=1.03 g cm^{-3}, d=0.05 mm for the small sample (m=2.5 mg) and d=0.5 mm for the large sample (m=25 mg); specific heat capacity of the sample supposed to be real valued. One can see that for the small sample there is negligible difference between specific heat capacity of the sample c_p and apparent specific heat capacity $c_\alpha = C_\alpha/m$ at any reasonable values of c_p. (Note that c_p which is usually in order of 1–2 J g^{-1} K^{-1} can increase in several times in the melting region due to latent heat.) Out of melting region for the large sample, apparent heat capacity has approximately the same absolute value as sample heat capacity, $|c_\alpha| \approx c_p$, and there is only small contribution on phase, $\arg(c_\alpha)$=0.06 rad. But situation can appreciably change in the melting region. If c_p increases up to 40 J g^{-1} K^{-1} (that is possible, e.g. for poly(ethylene caprolactone)), then $|c_\alpha| \approx 0.57 c_p$ and phase angle reaches the value 0.74 rad. And this is only at $t_{\rm p}$=1 min – the period normally used for TMDSC measurements.

Now include the influence from thermal contact between the sample and the pan, $K_{\rm ps}$. Heat flow rate from the pan to the sample (which equals to the heat flow rate into the sample) is $\Phi_{\rm p}(t) = K_{\rm ps}(T_{\rm p}(t) - T_{\rm s}(0,t))$. From that one can write: $T_{\rm p}(t) = T_{\rm s}(0,t) + (1/K_{\rm ps})\Phi_{\rm p}(t)$, $T_{\rm p}(t) = T_{\rm s}(0,t)(1 - (\mathrm{i}\omega/K_{\rm ps})C_\alpha)$, or $T_{\rm s}(0,t) = T_{\rm p}(t)/(1 - (\mathrm{i}\omega/K_{\rm ps})C_\alpha)$. Then Eq. (11) for heat flow rate $\Phi_{\rm p}(t)$ can be rewritten as

$$\Phi_{\rm p}(t) = -C_\beta \cdot \mathrm{i}\omega \cdot T_{\rm p}(t), \tag{13}$$

where C_β is the apparent heat capacity of the sample at aluminium pan surface, which can be calculated as

$$C_\beta \equiv \frac{C_\alpha}{1 - (\mathrm{i}\omega/K_{\rm ps})C_\alpha}. \tag{14}$$

Table 1

c_p (J g^{-1} K^{-1})	m=2.5 mg		m=25 mg	
	$\lvert c_\alpha\rvert$ (J g^{-1} K^{-1})	Arg(c_α) (rad)	$\lvert c_\alpha\rvert$ (J g^{-1} K^{-1})	Arg(c_α) (rad)
2	1.9999994	7×10^{-4}	1.995	0.06
10	9.99993	0.003	9.38	0.3
40	39.995	0.001	23	0.74

Fig. 2(a) shows C_β dependence on parameter ω/K_{ps}. Again at low frequency ω or at good thermal contact K_{ps}, i.e. at $\omega/K_{ps} \to 0$, $C_\beta \to C_\alpha$; at $\omega/K_{ps} \to \infty$ $C_\beta \to 0$ and $\arg(C_\beta) \to \pi/2$.

Using analogous algorithm one can calculate the heat flow rate into the pan, $\Phi_o(t)$:

$$\Phi_o(t) = -i\omega \cdot T_o(t) \frac{C_{pan} + C_\beta}{1 - (i\omega/K_{op})(C_{pan} + C_\beta)} = -C_\gamma \cdot i\omega \cdot T_o(t), \quad (15)$$

where C_{pan} is the heat capacity of aluminium pan (real valued) and C_γ is the apparent heat capacity of the sample–pan system, which can be calculated as

$$C_\gamma \equiv \frac{C_{pan} + C_\beta}{1 - (i\omega/K_{op})(C_{pan} + C_\beta)}. \quad (16)$$

C_γ dependence on parameter ω/K_{op} is analogous to that shown in Fig. 2(a) for C_β. At $\omega/K_{op} \to 0$, $C_\gamma \to C_{pan} + C_\beta$; at $\omega/K_{op} \to \infty$, $C_\gamma \to 0$ and $\arg(C_\lambda) \to \pi/2$.

In TMDSC, as well as in DSC, measured heat flow rate is the difference between total heat flow rates to the sample oven and to the reference oven. For simplicity, suppose that the reference oven is empty, then in ideal symmetrical case differential heat flow rate equals to the heat flow rate from the sample oven to the sample–pan system, $\Phi_o(t)$. In fact some asymmetry between these two ovens is inevitable, therefore measured heat flow rate, $\Phi_o^{p+s}(t)$, contains additional part, so that

$$\Phi_o^{p+s}(t) = -i\omega \cdot T_o(t) \times \frac{C_{pan} + C_\beta}{1 - (i\omega/K_{op})(C_{pan} + C_\beta)} + f(t), \quad (17)$$

where $f(t)$ is some additional function, describing asymmetry in heat leakage and in heat capacity of the ovens. This function, $f(t)$, is mainly determined by temperature oscillations of the ovens. Due to the power compensation and due to the fact that ovens heat capacities are roughly two orders of magnitude larger than sample plus pan heat capacity the temperature oscillations of the ovens are independent on measurements with or without sample. Therefore, under given temperature oscillations $f(t)$ is highly reproducible. Commonly for DSC and TMDSC heat flow rate of empty pan (C_β=0), $\Phi_o^p(t)$, is measured to determine the asymmetry function $f(t)$:

$$\Phi_o^p(t) = -i\omega \cdot T_o(t) \frac{C_{pan}}{1 - (i\omega/K_{op})C_{pan}} + f(t). \quad (18)$$

Then empty pan corrected heat flow rate, $\Phi_o^s(t)$, is calculated as difference between Eqs. (17) and (18):

$$\Phi_o^s(t) \equiv \Phi_o^{p+s}(t) - \Phi_o^p(t) = -C_\delta \cdot i\omega \cdot T_o(t), \quad (19)$$

where C_δ is the apparent heat capacity after empty pan correction, which equals

$$C_\delta \equiv \frac{C_\beta}{(1 - (i\omega/K_{op})(C_{pan} + C_\beta))(1 - (i\omega/K_{op})C_{pan})}. \quad (20)$$

Fig. 2(b) shows C_δ dependence on parameter ω/K_{op}. For given C_β the value of C_δ is also dependent on pan heat capacity C_{pan}. At $C_{pan} \to 0$ the shape of the curve tends to semi-circle as in Fig. 2(a) for vector C_β. Again at good conditions, i.e. at $\omega/K_{op} \to 0$, $C_\delta \to C_\beta$; at $\omega/K_{op} \to \infty$ $C_\delta \to 0$ and $\arg(C_\delta) - \arg(C_\beta) \to \pi$.

Now estimate the influence of thermal contact K_{op} on measured heat capacity value. For calculations by Eq. (20) assume that $C_\beta = m \cdot c_p$ that means there are negligible temperature gradient inside the sample and ideal thermal contact between sample and pan. Other parameters are the following: t_p=1 min, C_{pan}=29 mJ K^{-1}, K_{op}=30 mW K^{-1}. The value for K_{op} was taken from preliminary calibration with aluminium samples (see Section 5). The results for two different sample masses are shown in Table 2. One can see that even for small sample, m=2.5 mg, there is relatively large contribution in phase angle, $\arg(c_\delta)$=0.22 rad. It reflects the fact that by decreasing the sample mass one can decrease this thermal lag (difference between C_β and C_δ) only to a given limit determined by relatively large heat capacity of the sample pan. Moreover, for large sample in the melting region, contribution in phase angle from thermal contact between pan and oven can reach even 1.41 rad and modulus of apparent heat capacity can be four times smaller, $|c_\delta| = 0.25 c_p$. Note again, that this result is obtained for t_p=1 min – period that is supposed to be not short for 25 mg samples and is commonly used in TMDSC measurements.

Table 2

c_p (J g^{-1} K^{-1})	m=2.5 mg		m=25 mg	
	$\lvert c_\delta \rvert$ (J g^{-1} K^{-1})	Arg(c_δ) (rad)	$\lvert c_\delta \rvert$ (J g^{-1} K^{-1})	Arg(c_δ) (rad)
2	1.976	0.22	1.915	0.37
10	9.77	0.29	7.02	0.89
40	36	0.53	10.3	1.41

4. Calibration algorithm of heat transfer

Now summarise the results from the previous section. First, sample heat capacity $m{\cdot}c_p$, being measured on the sample surface, appears as C_α. Next, C_α, being measured on the pan surface, appears as C_β. After empty pan correction C_β, being measured on the surface of the oven, appears as C_δ. Table 3 shows how much the values c_α, c_β, c_δ can change for real measurements. The values for the parameters are the same as in Tables 1 and 2, K_{ps}=22 mW K^{-1}, m=25 mg.

C_δ, according to Eq. (19), can be calculated as

$$C_\delta = \frac{A_{\Phi^{\mathrm{s}}_{\mathrm{o}}}}{A_{q_{\mathrm{o}}}} \mathrm{e}^{\mathrm{i}\delta}, \tag{21}$$

where $A_{\Phi^{\mathrm{s}}_{\mathrm{o}}}$ is the amplitude of empty pan corrected heat flow $\Phi^{\mathrm{s}}_{\mathrm{o}}(t)$ and $A_{q_{\mathrm{o}}}$ is the amplitude of heating rate at oven surface $q_{\mathrm{o}}(t)=-\mathrm{i}\omega{\cdot}T_{\mathrm{o}}(t)$. Then the sample heat capacity $m{\cdot}c_p$ can be determined as

$$m \cdot c_p = \frac{m \cdot c_p}{C_\delta} \frac{A_{\Phi^{\mathrm{s}}_{\mathrm{o}}}}{A_{q_{\mathrm{o}}}} \mathrm{e}^{\mathrm{i}\delta} = B_1 \frac{A_{\Phi^{\mathrm{s}}_{\mathrm{o}}}}{A_{q_{\mathrm{o}}}} \mathrm{e}^{\mathrm{i}\delta}, \tag{22}$$

where complex factor $B_1 \equiv (m \cdot c_p)/C_\delta$ depends not only on frequency, but on all parameters which are in Eqs. (12), (14) and (20). The most crucial one is c_p for it just has to be measured. Therefore, it is impossible by any calibration procedure to determine the calibration factor B_1 in advance and then apply it to the sample measurements. But it is possible by calibration (see Section 5) to determine the thermal contact between oven and pan K_{op}. Then, knowing this thermal contact and pan heat capacity C_{pan} (which can be calculated or measured independently) one can get the value of C_β from C_δ, see Eq. (20). Further one can use, when it is possible, thin layer of a grease or an oil between pan and sample to improve thermal contact K_{ps} and keep it constant and independent on sample state. In this case, using the same thin layer of a grease or an oil in calibration, e.g. with aluminium disc inside the pan one can calculate the value of K_{ps}, see Eq. (14), where C_β is the measured value and C_α is the heat capacity of the aluminium disc, which can be measured or calculated independently. Further, knowing the value of K_{ps}, one can determine by Eq. (14) the value of C_α from C_β for sample measurement. Then the last step is to get by Eq. (12) the value of c_p from C_α. Here one can face the problem that specific heat capacity c_p is coupled with thermal conductivity κ_{s} and it can be difficult to separate these two unknown values from one calculated value of C_α. But one can calculate two values of C_α from two different measurements of the same compound, e.g. for the first measurement use a sample with effective thickness d and for the second measurement use two times thicker sample. As long as all other parameters are the same, from Eq. (12) one can write

$$\frac{C_\alpha(2d)}{C_\alpha(d)} = \frac{\tanh(2\alpha \cdot d)}{\tanh(\alpha \cdot d)}, \tag{23}$$

where $C_\alpha(2d)$ and $C_\alpha(d)$ denote apparent heat capacity C_α for the sample with effective thickness $2d$ and d, respectively. Then knowing the complex value of $\alpha{\cdot}d$ from Eq. (23) one can determine by Eq. (12) sample

Table 3

c_p (J g^{-1} K^{-1})	$\lvert c_\alpha \rvert$ (J g^{-1} K^{-1})	Arg(c_α) (rad)	$\lvert c_\beta \rvert$ (J g^{-1} K^{-1})	Arg(c_β) (rad)	$\lvert c_\delta \rvert$ (J g^{-1} K^{-1})	Arg(c_δ) (rad)
2	1.995	0.06	1.91	0.30	1.75	0.65
40	23.25	0.74	6.43	1.36	4.04	1.60

thermal conductivity, κ_s. Finally, from the values of κ_s and of $\alpha \cdot d = \sqrt{(\omega/|\chi|)}\exp\{(i/2)\arg(-i\omega/\chi)\}d$, where $\chi = \kappa_s/(\rho \cdot c_p)$, one can determine sample specific heat capacity c_p. Here, one can get the value of sample density ρ from hand-book or measure directly. However, some problems can appear when the sample density appreciable changes with temperature or with time (e.g. during quasi-isothermal crystallisation). Any expansion or contraction of the sample can lead not only to the density change but obviously to some changes in sample effective thickness d and contact area S (and therefore to some changes in thermal contact between pan and sample K_{ps} as well). Then, if necessary, the value of ρ or of expansion coefficient can be independently measured under the same time–temperature conditions as in TMDSC experiments. After that one can estimate by Eqs. (12) and (14) the influence of this expansion or contraction on calculated value of sample heat capacity c_p.

5. Calibration of apparatus influence

One kind of apparatus influence (inevitable asymmetry of the ovens) has been already discussed in Section 3. In the previous section we used the fact that measured temperature is the temperature of the oven surface. In reality temperature is measured inside the oven. Another fact is that temperature signal is used in a feed-back controller for power compensation and to calculate the heat flow rate signal, so that the measured heat flow rate after empty pan correction $\Phi^s(t)$ also differs from heat flow rate $\Phi^s_o(t)$. As shown in [11] connection between $\Phi^s(t)$ and $\Phi^s_o(t)$ and between measured temperature and oven surface temperature can be described by convolution product with Green's functions. Similar way like in Eqs. (2)–(5) one can show that Eq. (21) can be rewritten as

$$C_\delta = \frac{A_{\Phi^s_o}}{A_{q_o}} e^{i\delta} = B_2(\omega)\frac{A_{\Phi^s}}{A_q} e^{i\epsilon}, \qquad (24)$$

where $B_2(\omega) = (A_{\Phi^s_o}/A_{\Phi^s})(A_q/A_{q_o})e^{i(\delta-\epsilon)}$ is some complex factor that describes apparatus influence on measured value of C_δ. In spite of the fact that this factor has contribution also from heat transfer inside the oven, it is assigned to the apparatus influence because the key difference of this factor from factor B_1 is independent on sample heat capacity. Then, it is possible without going into details of measuring system and electronics, to calibrate this apparatus influence. For example, at a given temperature and frequency one can measure two aluminium discs with the same diameter but different thickness. For simplicity one can use empty oven correction (not empty pan), that means use empty oven measurement to determine the asymmetry function $f(t)$. After such correction apparent heat capacity C_γ is measured, where now in Eq. (17) $C_{pan}+C_\beta$ equals heat capacity of an aluminium disc C_{Al}. One can write

$$C_\gamma \equiv \frac{C_{Al}}{1-(i\omega/K_{op})C_{Al}} = B_2(\omega)\frac{A_{\Phi^o}}{A_q} e^{i\epsilon}, \qquad (25)$$

where A_{Φ^o} is the amplitude of measured heat flow rate after empty oven correction, A_q the amplitude of measured heating rate, and ϵ is the phase angle between these heating rate and heat flow rate. For two different aluminium discs with heat capacities C_{Al1} and C_{Al2} one can write from Eq. (25):

$$\frac{C_{\gamma 1}}{C_{\gamma 2}} \equiv \frac{1-(i\omega/K_{op})C_{Al2}}{1-(i\omega/K_{op})C_{Al1}}\frac{C_{Al1}}{C_{Al2}} = \frac{A_{\Phi^o_1}}{A_{\Phi^o_2}}\frac{A_{q_2}}{A_{q_1}} e^{i(\epsilon_1-\epsilon_2)}. \qquad (26)$$

From this ratio one can determine the thermal contact between oven and aluminium discs K_{op} and by Eq. (25) determine the value for $B_2(\omega)$. One can use more than two discs to increase the accuracy in determination of $B_2(\omega)$. Fig. 3 shows the result of such correction. By Eq. (26) thermal contact K_{op} has been determined (K_{op}=45 mW K^{-1}), and by Eq. (25) the calibration factor $B_2(\omega)$ has been calculated. The application of the calibration $c_\gamma = c_{eff}\,B_2(\omega)$ leads to changes in argument and modulus of apparent heat capacity in such way that vectors c_γ on polar plot lie on semi-circle. This behaviour of c_γ is fully described by thermal contact between the disc and the oven K_{op} (in our definition K_{op} is the thermal contact between sample pan and oven, but aluminium discs were measured directly in the oven without any pan). Then after correction on K_{op}, see Eq. (25), all vectors $c_p(\omega)$ will coincide with real valued c_p(Al). (As one can estimate by Eq. (12), for the thickest disc at the highest frequency thermal conductivity of aluminium contributes only 0.025 rad in argument of apparent heat capacity c_α, i.e. $c_\alpha \approx c_p$(Al)) Remarkable in

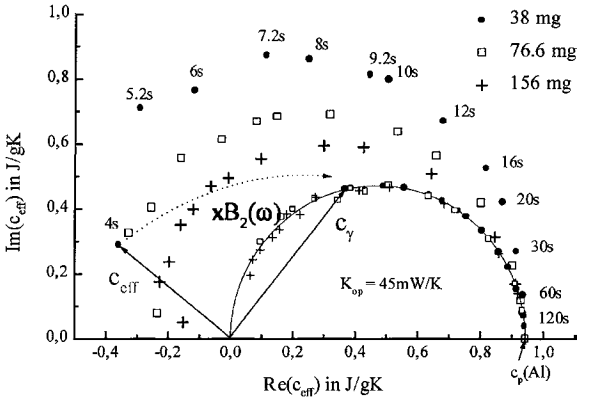

Fig. 3. Effective specific heat capacity of aluminium c_{eff}, determined by Eq. (1), at different modulation periods (t_{p}=4–120 s) and for different sample masses. Aluminium discs with diameter 6 mm and thickness 0.5 mm (m=38 mm), 1 mm (m=76.6 mm) and 2 mm (m=156 mm), respectively, have been measured by Perkin-Elmer DSC Pyris 1, T_0=443 K, saw-tooth temperature oscillations. Small arrow at real axis indicates the value for specific heat capacity of aluminium, c_p(Al)=0.944 J g^{-1} K^{-1}, obtained by common DCS scan with q_0=5 K min^{-1}.

Fig. 3 is the fact that after calibration on the same factor $B_2(\omega)$ really all vectors $c_\gamma=C_\gamma/m$ of all three discs at all frequencies lie within experimental uncertainties on semi-circle. This means that calibration factor $B_2(\omega)$ really does not depend on sample heat capacity. The values for modulus and argument of $B_2(\omega)$ at different frequencies are shown in Fig. 4. Knowing $B_2(\omega)$ one can further measure standard aluminium pans to determine by Eq. (25) corresponding value of K_{op}. As an example from preliminary study K_{op} for standard aluminium pans equals 30 mW K^{-1} at 170°C. The value for K_{op} is highly reproducible and not sensitive to some non-coaxial position of the pan in the oven.

6. Discussion

At any TMDSC measurements, even at large periods there is a difference between sample heat capacity $m{\cdot}c_p$ and measured apparent heat capacity C_δ at least in phase angle. Therefore correction of measured data is necessary in any case. One cannot escape the need of correction using very small thin samples because large contribution from the sample pan cannot be excluded this way.

Since calibration factor B_1 depends on sample heat capacity it is not correct to use the value of B_1 determined, e.g. in the melted or in crystal state for the correction in the melting region, where c_p value can be quite different. One should be cautious by making different kinetic models of melting for experimental data one cannot thoroughly correct.

One should also be careful by checking with different sample masses how good is some calibration algorithm. If samples differ only by contact area S but have the same thickness, the same result from different sample masses can be obtained even in case when correction includes only apparatus influence and thermal contact between oven and pan. In this case one calculates after such correction something like apparent specific heat capacity $c_\beta=C_\beta/m$ which can be still far from sample specific heat capacity c_p.

Sometimes one measures samples of the same mass but with different thickness. Then the differences in the results for apparent heat capacity one assigns to the evidence of temperature gradient inside the sample.

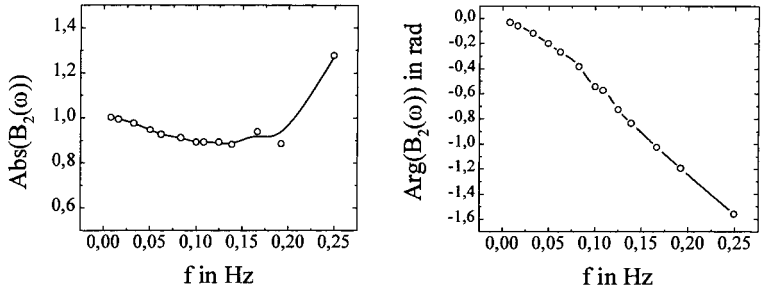

Fig. 4. Modulus and argument of calibration factor $B_2(\omega)$ at different frequencies of temperature modulation.

But these samples have different contact area S and therefore have different effective thermal contact with pan K_{ps} even when specific thermal contact per unit area is the same. In this case the result will be different for different samples with the same mass even when there is no temperature gradient inside the samples.

7. Conclusion

One can see that specific heat capacity determination by TMDSC measurements is influenced by many factors, among them the most important are the calibration factor of the instrument itself, $B_2(\omega)$, thermal contact between oven and pan, K_{op}, thermal contact between pan and sample, K_{ps}. Calibration factor of the instrument can be determined in advance, because it is independent on sample being measured. But one cannot determine by any calibration procedure in advance the influence of thermal contacts K_{op} and K_{ps} in sample measurements. Only using well-defined geometry of the sample and the pan and keeping these thermal contacts reproducible from measurement to measurement, one can determine specific heat capacity and thermal conductivity of the low heat conducting materials at any sample state. The upper frequency limit will be restricted by experimental accuracy in determination of these thermal contacts and apparatus factor $B_2(\omega)$. In case of high thermal conducting materials it is already possible to enlarge upper frequency limit of TMDSC measurements up to 0.25 Hz and sufficiently improve the accuracy of the measurements.

This theoretical part will be followed by experimental results of low thermal conducting materials based on presented correction algorithm.

Acknowledgements

This work was financially supported by European Commission, Grand no. IC15CT960821. The authors gratefully acknowledge discussions with G.W.H. Höhne, J.E.K. Schawe (University of Ulm, Germany) and A.A. Minakov (General Physic Institute, Moscow, Russia).

References

[1] P. Sullivan, G. Seidel, Ann. Acad. Sci. Fennicae A VI (1966) 58.
[2] P. Sullivan, G. Seidel, Phys. Rev. 173 (1968) 679.
[3] Y.A. Kraftmakher, Compendium of Thermophysical Property Measurement Methods, vol. 1, Plenum press, New York, 1984, p. 591.
[4] N.O. Birge, S.R. Nagel, Phys. Rev. Lett. 54 (1985) 2674.
[5] N.O. Birge, S.R. Nagel, Phys. Rev. B-Condensed Matter 34 (1986) 1631.
[6] M. Reading, Trends Polym. Sci. 8 (1993) 248.
[7] J.E.K. Schawe, Thermochim. Acta 261 (1995) 183.
[8] Y.H. Jeong, I.K. Moon, Phys. Rev. B 52 (1995) 6381.
[9] M. Merzlyakov, C. Schick, this volume.
[10] B. Wunderlich, Y. Jin, A. Boller, Thermochim. Acta 238 (1994) 277.
[11] J.E.K. Schawe, W. Winter, Thermochim. Acta 298 (1997) 9.
[12] I. Hatta, S. Muramatsu, Jpn. J. Appl. Phys 35 (1996) 858.
[13] B. Schenker, F. Stäger, Thermochim. Acta 304/305 (1997) 219.
[14] A.A. Lacey, C. Nikolopoulos, M. Reading, J. Therm. Anal. 50 (1997) 279.
[15] S. Weyer, A. Hensel, C. Schick, Thermochim. Acta 304/305 (1997) 267.
[16] B. Wunderlich, Y. Jin, A. Boller, Thermochim. Acta 238 (1994) 277.
[17] V.S. Vladimirov, Equations of Mathematical Physics, New York, Dekker, 1971.
[18] J.E.K. Schawe, C. Schick, G.W.H. Höhne, Thermochim. Acta 229 (1993) 37.